Enhancing Texture Analysis by Color Shading Correction

Christian Münzenmayer[1], Frederic Naujokat[1], Steffen Mühldorfer[2], and Thomas Wittenberg[1]

[1] Fraunhofer Institut für Integrierte Schaltungen,
Am Wolfsmantel 33, D-91058 Erlangen
mzn@iis.fraunhofer.de
[2] Universität Erlangen-Nürnberg, Medizinische Klinik I,
Ulmenweg 18, D-91054 Erlangen

Abstract

The automated analysis and classification of textured regions in color images is an active field of research in image processing and pattern recognition. However, most of the published algorithms require ideal imaging conditions with respect to homogenous illumination conditions or calibrated recording devices. In this work we propose a YUV-based shading correction technique applicable to color images. Experiments conducted on images with synthesized shading show feasibility of the approach. Moreover the application of our algorithm to endoscopic images of the esophagus show significant gains in classification performance.

1 Introduction

The automated analysis and classification of textured regions in color images is an active field of research in image processing and pattern recognition. However, most of the published algorithms require ideal imaging conditions with respect to homogeneous illumination conditions or calibrated recording devices. For example, real world applications in industrial or medical environments have to deal with changing light source characteristics due to aging and inhomogeneous illumination due to geometry constraints. Publications dealing with the problem of retrospective shading correction generally consider gray level images only and do not provide adequate solutions for color images [TLP00, Jäh02, LMVP00]. Furthermore, no results are available how such pre-processing methods may influence subsequent texture analysis.

One application example, where illumination correction is needed, is the analysis of high-resolution color images obtained by magnification video-endoscopes. Such endoscopes are also used for screening patients with chronic gastroesophageal reflux disease which results in about 5% of cases to so-called Barrett's esophagus. This is a pre-malignant epithelium that builds up in consequence of inappropriate repair of esophageal injury due to chronic reflux [Fen00]. About one to two percent of the adult population in the United States are assumed to have Barrett's esophagus, explaining the large increase of the incidence of esophageal adenocarcinoma, the Barrett's associated cancer, in the last thirty years [Fen00]. The distinction between benign tissue of the Cardia and Barrett's esophagus is a difficult problem in endoscopy and still requires conventional biopsy with following histology. The state of the art still is the "random-biopsy", taking samples from all four quadrants of the considered section of the esophagus. A long-term goal of our research is to support the examiner by an intelligent endoscope which helps in detecting and classifying the tissue in

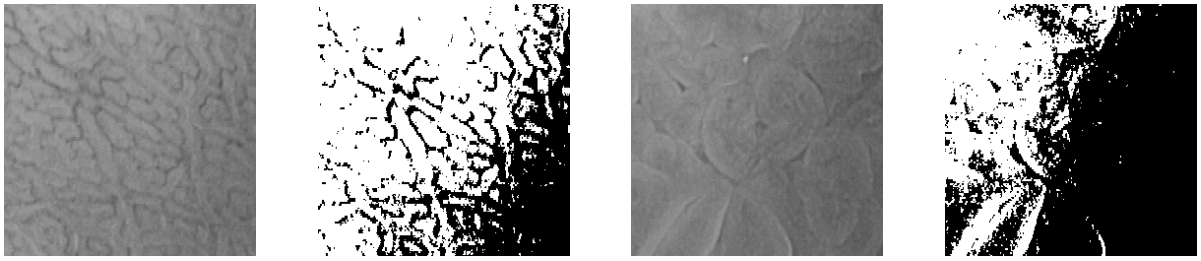

(a) Corpus tissue (b) Global thresholding (c) Cardia tissue (d) Global thresholding

Figure 1: Endoscopic images show illumination gradient to the right bottom corner which leads to unacceptable results with a simple global thresholding. Texture features relying at least partially on absolute intensities will misbehave with such kind of data.

the field of view. Such CAD[3] systems are expected to help directing a faster biopsy with fewer samples and giving an objective "second opinion".

2 Gray Level Shading Correction

The problems caused by inhomogenous illumination conditions in automated image analysis have been a known problem in the image processing community for the last decades. Shading or intensity inhomogeneities often show slowly decreasing intensity over an image. The human visual system automatically compensates for this effect, which in contrast is not quite possible with computer vision systems as depicted in Figure 1 for the case of a simple global thresholding operation. In the literature the relation between an assumed shading-free image $U(x, y)$ and the image $N(x, y)$ which is acquired by a real camera has been formulated with a linear model [TLP00]:

$$N(x, y) = U(x, y)S_M(x, y) + S_A(x, y) \tag{1}$$

The components $S_M(x, y)$ and $S_A(x, y)$ are image location dependent multiplicative and additive shading components, respectively, which are generally unknown. In a standardized image acquisition setting a set of two reference images can usually be used to obtain an estimate for the shading-free image $U(x, y)$. With a black image $B(x, y)$ accounting for the dark current of the CCD-chip in the camera and a white image $W(x, y)$ acquired by recording a homogenous white image below the clipping level of the camera, an estimate $\hat{U}(x, y)$ can be found using [Jäh02]:

$$\hat{U}(x, y) = C\frac{N(x, y) - B(x, y)}{W(x, y) - B(x, y)} \tag{2}$$

However, it can be seen that this approach has its limitations even under a controlled image acquisition setting as medical endoscopy. This is because object-dependent shading can not be compensated for with reference image approaches and therefore we require so-called retrospective shading correction methods. By definition these algorithms estimate the shading components solely by means of the acquired image $N(x, y)$. Assuming that shading is located in the low frequency domain below the image content of interest, linear and homomorphic filtering techniques can be used. Linear filtering cares only for the additive shading component $S_A(x, y)$ which is estimated by low-pass filtering (LPF) [TLP00]:

$$\hat{S}_A(x, y) = \mathrm{LPF}\{(N(x, y))\} \tag{3}$$

[3]Computer Aided Diagnosis

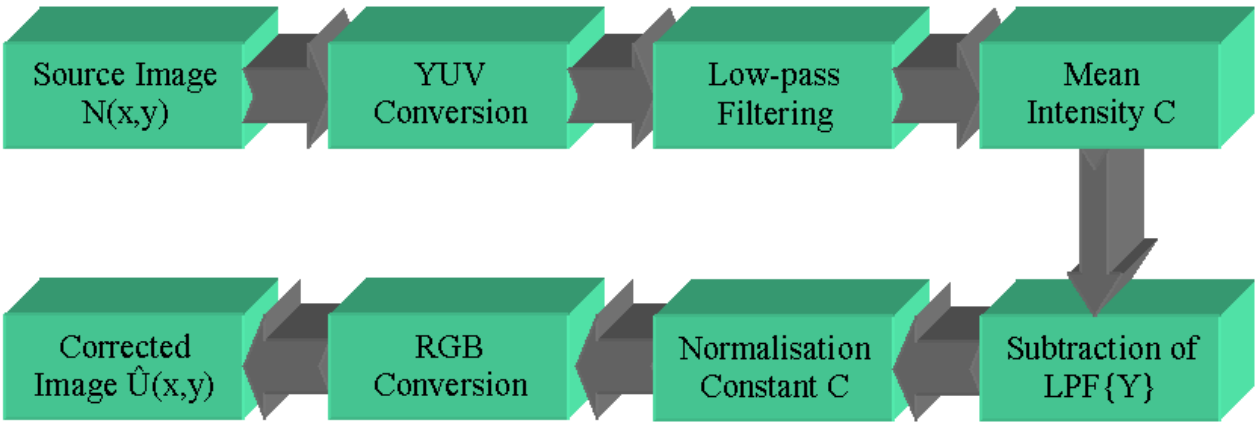

Figure 2: Processing in the YUV Smoothing Algorithm. Images are separated into luminance and chrominance information, luminance is corrected by standard shading correction methods and afterwards an inverse conversion is performed.

leading to the simple estimate of the shading-free image

$$\hat{U}(x,y) = N(x,y) - \hat{S}_A(x,y) + C \tag{4}$$

where the normalization constant C can be computed as the mean gray level of the shading estimate $C = E\{\hat{S}_A(x,y)\}$. Note that multiplicative shading components are neglected in this approach. This can be handled by homomorphic filtering algorithms which involve low-pass filtering of the logarithm of images by exploiting the relation

$$\log\{N(x,y)\} = \log\{U(x,y)\} + \log\{S_M(x,y)\} \tag{5}$$

in this case neglecting the additive shading component $S_A(x,y)$. A similar technique is using morphological filtering to estimate the shading components. More complex approaches are trying to fit a shading model applying second order polynomials on some pre-selected points [TLP00]. A recent paper by Likar et al. [LMVP00] also uses second-order polynomials for modeling of the shading-components but optimizes the coefficients by minimisation of the entropy $H\{\hat{U}(x,y)\}$.

3 Color Shading Correction

However, the described approaches concentrate solely on the use of gray-level images. Therefore, the question arises, how they can be used on color images which are of increasing concern in research and development today. A straight-forward extension for color images applies the gray level linear filtering to every plane of an RGB image independently. This method shall be refered to as *intra-plane smoothing*. Due to the combined encoding of intensity and chromaticity in the RGB image this filtering technique might influence color information in uncontrolled and undesireable ways.

In the process of color image shading correction it is therefore desirable to correct only the intensity information. Suitable color spaces to separate chromaticity from intensity information are the family of HSI[4] color models or color difference spaces such as YUV [PV00].

[4]Hue, Saturation, Intensity

The YUV color space consists of the luminance channel Y and the chrominance channels U and V and is linearly related to the device RGB values by a matrix transform

$$\begin{pmatrix} Y \\ U \\ V \end{pmatrix} = \begin{pmatrix} 0.299 & 0.587 & 0.114 \\ -0.147 & -0.289 & 0.437 \\ 0.615 & -0.515 & 0.100 \end{pmatrix} \begin{pmatrix} R \\ G \\ B \end{pmatrix} \tag{6}$$

with the respective inverse transform left out for the sake of brevity here. Our correction algorithm therefore starts with the conversion of the acquired RGB image $N_{\mathrm{RGB}}(x, y)$ to its YUV representation $N_{\mathrm{YUV}}(x, y)$ by applying (6):

$$N_{\mathrm{RGB}}(x, y) \xrightarrow{\mathrm{YUV}} N_{\mathrm{YUV}}(x, y) \tag{7}$$

For correction purposes only the intensity channel Y denoted by $N^{(Y)}_{\mathrm{YUV}}(x, y)$ is used, leading to the corrected intensity channel of the estimate $\hat{U}_{\mathrm{YUV}}(x, y)$ as

$$\hat{U}^{(Y)}_{\mathrm{YUV}}(x, y) = N^{(Y)}_{\mathrm{YUV}}(x, y) - \mathrm{LPF}\{N^{(Y)}_{\mathrm{YUV}}(x, y)\} + C \tag{8}$$

where C is the mean intensity of the low-pass filtered Y channel. the color difference signals U and V are taken unchanged from the original image in YUV representation

$$\hat{U}^{(U,V)}_{\mathrm{YUV}}(x, y) = N^{(U,V)}_{\mathrm{YUV}}(x, y). \tag{9}$$

After back-conversion by the inverse transformation of (6)

$$\hat{U}_{\mathrm{YUV}}(x, y) \xrightarrow{\mathrm{YUV}^{-1}} \hat{U}_{\mathrm{RGB}}(x, y) \tag{10}$$

the corrected estimate $\hat{U}_{\mathrm{RGB}}(x, y)$ can be used for further processing. The whole procedure is shown in Figure 2 and will be called *YUV smoothing* throughout the rest of the paper. It is quite obvious that any gray level algorithm might be used for color images in this way which is just a matter of implementation.

4 Experiments And Results

4.1 Artifical Shadows

The evaluation of the proposed shading correction scheme is performed in two contexts. At first we show experiments with artificial shadows on a known image where we have known ground truth about the ideal image $U(x, y)$. Secondly, we work with real color images from medical endoscopy.

For our experiments with ground truth we use the famous Lena image (see Figure 4(a)) which has been modified by an additive linear shading (see Figure 4(b)). To avoid clipping of gray levels after adding of the shading components each intensity value was divided by two.

For evaluation purposes we used different filter sizes for the low-pass filter and computed the root mean square error (RMSE) and the normalized cross correlation (NCC) between the original image $U(x, y)$ and the corrected estimate $\hat{U}(x, y)$ (Table 1). To handle the relatively large filter sizes for background estimation we used an iterative implementation of a binomial filter. The reference RMSE and NCC between the original image U(x,y) and the uncorrected shaded image N(x,y) is 76.2831 and 0.9503, respectively.

It can be seen from this table that the values of the RMSE decrease while the values of the NCC increase with increasing filter size until they reach a minimum and maximum at a

Table 1: Influcence of filter size on root mean square error (RMSE) and normalized cross correlation (NCC) for intra-plane and YUV smoothing. The reference RMSE and NCC between the original image U(x,y) and the uncorrected shaded image N(x,y) is 76.2831 and 0.9503, respectively.

Filter Size	RMSE (intra)	NCC (intra)	RMSE (YUV)	NCC (YUV)
31	81.4775	0.9434	81.6647	0.9434
51	78.7138	0.9474	78.9625	0.9474
101	71.5738	0.9572	71.1825	0.9581
151	65.4339	0.9646	65.3125	0.9653
201	62.8902	0.9674	62.1392	0.9687
251	61.6267	0.9686	60.4998	0.9706
301	61.8268	0.9681	**60.0480**	**0.9706**
351	63.2623	0.9663	61.4447	0.9688

filter size of 301, respectively. This result is in agreement with expectations as shadows are assumed to be of low frequency. At its minimum the RMSE is still far from being neglectable with a value of about 60. This is a matter of applicability of the RMSE to illumination correction as these algorithms try to distribute the intensity homogenously over the image via the constant C but do not completely remove it.

What is also visible is that the YUV smoothing performs only slightly better in terms of these measures for this example. However, this was expected as our simulated shadow was created by adding a linear ramp to each of the RGB channels.

Figure 4(c) shows the result of applying YUV shading correction with a filter size of 301. The successful elimination of the intensity gradient is visible and emphasized by the corresponding line profiles shown in Figure 4(d)-4(f). These RGB line profiles are extracted at the height of the eyes of Lena.

One problem that still remains, is that the absolute intensity level is difficult to recover in such experiments. As every image acquisition inherently depends on the amount of light in the scene we consider it an acceptable rule to distribute the intensity by a constant offset C in the scene, see equ. (8).

4.2 Inhomogenous Endoscopic Images

Inhomogeneous illumination is an inherent problem in medical endoscopy. In our case we used a flexible zoom-endoscope with a CCD-chip at the distal end (Olympus GIF Q160Z, see Figure 3(a)). It allows imaging with up to 115× optical magnification with a depth of view between 1.5mm and 3.0mm. However, the two light sources beneath and above the camera window lead to an inhomogeneous lighting in the field of view (see details in Figure 3(b)).

We evaluated our results on an image database of 167 endoscopic images of the esophagus bearing strong illumination gradients. These are true color images (768×576) which have been acquired in 115× zoom mode from 35 patients. Within these images 176 irregular regions have been labeled manually with one of four tissue classes which were confirmed by two experienced pathologists after conventional biopsy. We considered benign epithelium, mucosa of the Cardia and the Corpus and of course different stages of neoplasia (Barrett).

Automatic classification of these regions was done using a selection of eight color texture algorithms and a nearest neighbor classifier used in a leaving-one-out scheme. The features used are color histograms, co-occurrence features [HSD73] and color-enabled versions of the

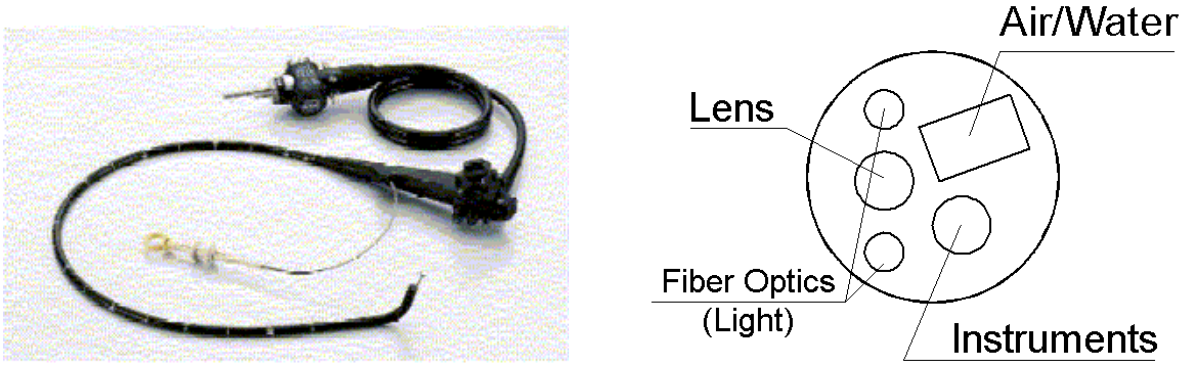

(a) Olympus GIF Q160Z

(b) Arrangement of light sources and camera

Figure 3: Olympus GIF Q160Z flexible magnification endoscope with distal chip camera. The arrangement of light sources and camera leads to inhomogeneous lighting in the field of view.

Table 2: Best Classification rates **r** and corresponding filter size **N** show the improvements by shading correction methods. For each algorithm the best result from a set of filter sizes $N \in 3, 15, 51, 101, 151, 201$ is shown. The texture features used are described in [HSD73, MVK+02, MVP+02].

	-	Reference	Intra-plane		YUV	
Features	$\mathbf{r_0}$	$\mathbf{r_{Ref}}$	$\mathbf{r_{Int}}$	**N**	$\mathbf{r_{YUV}}$	**N**
Color Histograms	64%	69%	68%	151	**70%**	201
Inter Plane S/D	64%	**72%**	71%	151	**72%**	201
Gray Level S/D	67%	66%	**72%**	51/151	66%	101/151
SGF Gray	55%	65%	68%	101	**71%**	151
SGF I1I2I3 16	62%	**68%**	63%	201	66%	201
SGF XOR 16	71%	**76%**	72%	201	74%	51
SGF XOR 4	72%	72%	72%	151/201	**75%**	101
Co-occurrence	69%	61%	**72%**	151	67%	201
Mean Improvement	-	3%	4%	-	5%	
Maximal Improvement	-	10%	13%	-	16%	

sum- and difference-histograms (S/D) [MVK+02] and statistical geometrical features (SGF) [MVP+02].

We compare the classification rates of the *intra-plane* and the *YUV* shading correction method with the results of the *reference image* based correction according to (2) and without any preprocessing. The improvement in classification rates serves as another evaluation measure for our algorithms. For each algorithm the best result from a set of filter sizes $N \in \{3, 15, 51, 101, 151, 201\}$ is shown in Table 2.

We achieved a mean absolute improvement in classification rates r of 4% for the intra-plane smoothing with up to 13% maximum improvement, depending on the filter size N. With 5% mean and 16% maximum improvement, even better results could be obtained by the YUV smoothing technique. A final comparison with a calibration image based approach only led to 3% mean and 10% maximum improvement, respectively (see Table 2).

Figure 5 show a representative result of our algorithm applied to an endoscopic image from our database. From regarding the horizontal profile lines in Figure 5(d)-5(f) the intra-plane

smoothing method seems to remove the shading artifacts better. However, as can be seen from the comparison of Figure 5(b) and 5(c), the intra-plane method introduces significant color artifacts which may be the case for the degradation in classification performance as well. Therefore, despite not being able to remove the shading completely we would prefer the YUV smoothing algorithm for its superior color reproduction.

5 Conclusion

It can be shown that even for an environment, where a controlled illumination is used, the reference image based method does not improve automatic classification significantly. That means the shading effects in gastroesophageal magnification endoscopy are scene dependent to a significant degree. The improvements in classification show a promising trend applying shading correction methods in color space. Future work may clarify how more complex shading correction methods e.g. based on fitting of polynomial shading models or entropy minimisation methods can be used on color images.

References

[Fen00] M. B. Fennerty. Chromoscopy in the diagnosis and management of barrett's esophagus. In M. Jung and J. F. Riemann, editors, *Internationales Symposium Chromoendoskopie*, pages 40–46, Mainz, 2000.

[HSD73] R. M. Haralick, K. Shanmugam, and I. Dinstein. Textural features for image classification. *IEEE Transactions on Systems, Man, And Cybernetics*, SMC-3(6):610–621, November 1973.

[Jäh02] B. Jähne. *Digitale Bildverarbeitung*. Springer-Verlag, Berlin Heidelberg, 5. edition, 2002.

[LMVP00] B. Likar, J.B.A. Maintz, M.A. Viergever, and F. Pernus. Retrospective shading correction based on entropy minimization. *Journal of Microscopy*, 197(3):285–295, 2000.

[MVK+02] C. Münzenmayer, H. Volk, C. Küblbeck, K. Spinnler, and T. Wittenberg. Multispectral texture analysis using interplane sum- and difference-histograms. In Luc Van Gool, editor, *Pattern Recognition - Proceedings of the 24th DAGM Symposium Zurich, Switzerland, September 2002*, pages 25–31, Berlin, 2002. Springer.

[MVP+02] C. Münzenmayer, H. Volk, D. Paulus, F. Vogt, and Wittenberg. Statistical geometrical features for texture analysis and classification. In *8. Workshop Farbbildverarbeitung, Autorenvorträge*, pages 87–94, Ilmenau, 2002. Zentrum für Bild- und Signalverarbeitung e.V. Ilmenau.

[PV00] K. N. Plataniotis and A. N. Venetsanopoulos. *Color Image Processing and Applications*. Springer-Verlag, Berlin, 1. edition, 2000.

[TLP00] D. Tomazevic, B. Likar, and F. Pernus. A comparison of retrospective shading correction techniques. In *International Conference on Pattern Recognition (ICPR'00)*, volume 3, pages 564–567. IEEE, 2000.

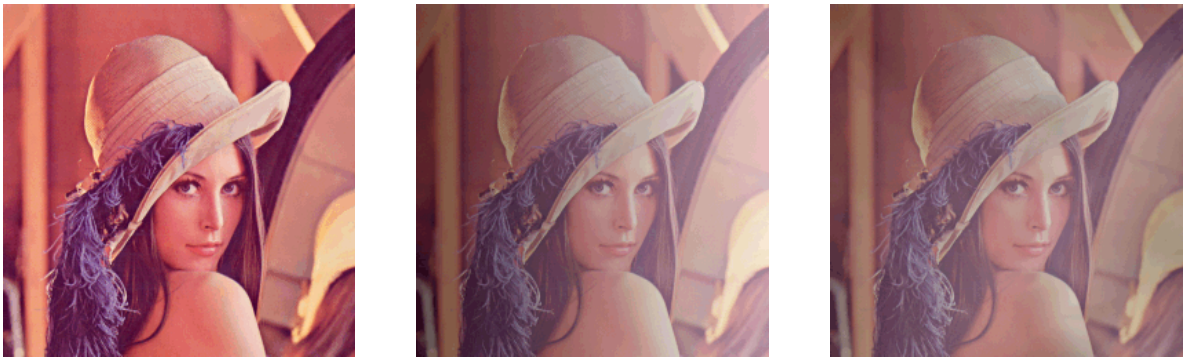

(a) The Famous Lena (b) Additive Linear Shading (c) YUV Smoothing

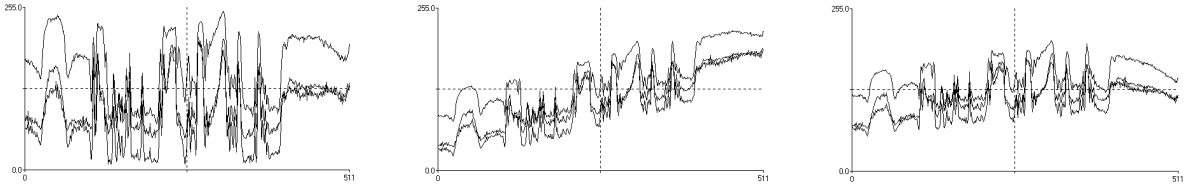

(d) RGB Line Profile (e) RGB Line Profile (f) RGB Line Profile

Figure 4: Illustration of the YUV shading correction on the Lena image. Figure (a) shows the well-known Lena image (b) additive linear shading was applied and (c) corrected with YUV smoothing with a filter size of 301. Figure (d-f) show the corresponding horizontal RGB line profiles at the height of the eyes of Lena.

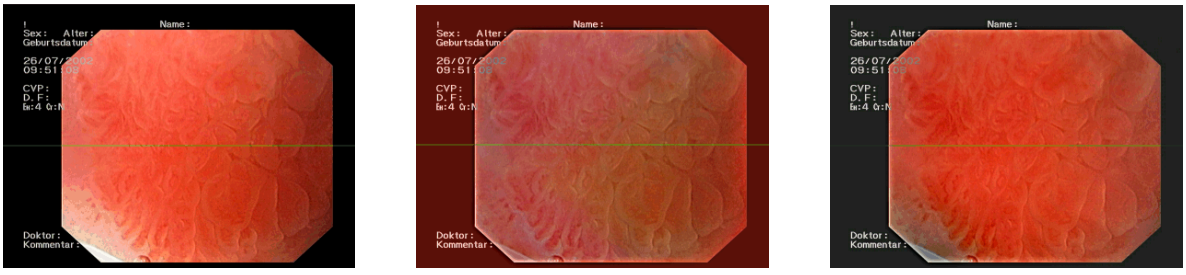

(a) Original Endoscopic Image (b) Intra-Plane Smoothing (c) YUV Smoothing

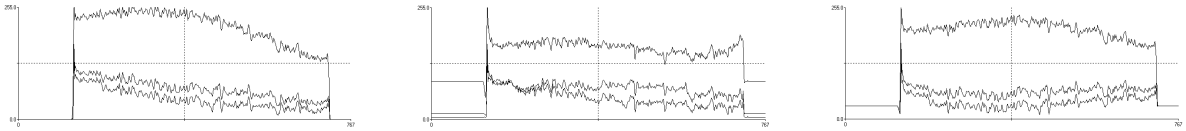

(d) RGB Line Profile (e) RGB Line Profile (f) RGB Line Profile

Figure 5: Illustration of the intra-plane and YUV shading correction on a real endoscopic image from our image database. Figure (a) shows the original image with strong gradient to the bottom right corner, (b) and (c) show the same image with intra-plane and YUV smoothing applied with filter size 201, respectively. Only slightly visible in print but noteworthy are significant color artifacts with the intra-plane approach. Figure (d-f) show the corresponding horizontal RGB line profiles at the center of the image.